Available on CMS information server

CMS NOTE -2012/001

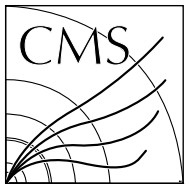

The Compact Muon Solenoid Experiment

CMS Note

Mailing address: CMS CERN, CH-1211 GENEVA 23, Switzerland

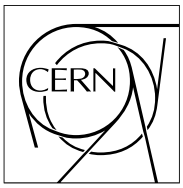

22 May 2012 (v2, 11 June 2012)

Tests of CMS Hadron Forward Calorimeter Upgrade Readout Box Prototype

The CMS HCAL Collaboration

Yerevan Physics Institute, Yerevan, Armenia
S. Chatrchyan, V. Khachatryan, A.M. Sirunyan, A. Tumasyan

National Centre for Particle and High Energy Physics, Minsk, Belarus
V. Mossolov, N. Shumeiko

Universiteit Antwerpen, Antwerpen, Belgium
T. Cornelis, S. Ochesanu, B. Roland, Z. Staykova, H. Van Haevermaet, P. Van Mechelen, A. Van Spilbeeck

Centro Brasileiro de Pesquisas Fisicas, Rio de Janeiro, Brazil
G.A. Alves, T. Martins, M.E. Pol, M. Vaz

Universidade do Estado do Rio de Janeiro, Rio de Janeiro, Brazil
W.L. Alda Junior, W. Carvalho, J. Chinellato, C. De Oliveira Martins, D. Matos Figueiredo, E. Manganote, J. Molina, L. Mundim, H. Nogima, W.L. Prado Da Silva, A. Santoro, A. Zachi

Charles University, Prague, Czech Republic
M. Finger, M. Finger Jr.

Institute of High Energy Physics and Informatization, Tbilisi State University, Tbilisi, Georgia
Z. Tsamalaidze[1]

Deutsches Elektronen-Synchrotron, Hamburg, Germany
K. Borras, P. Gunnelini, H. Jung[2], A. Knutsson, B. Lutz, P.M. Ribeiro Cipriano, N. Sen

Institute fur Experimentelle Kernphysik, Karlsruhe, Germany
C. Baus, I. Katkov[3], R. Ulrich, H. Wohrmann

University of Athens, Athens, Greece
A. Panagiotou

KFKI Research Institute for Particle and Nuclear Physics, Budapest, Hungary
G. Bencze, D. Horvath[4]

Panjab University, Chandigarh, India
S.B. Beri, R. Gupta, M. Jindal, M. Kaur, N. Nishu, L.K. Saini

Saha Institute of Nuclear Physics, Kolkata, India
S. Banerjee, S. Bhattacharya, B. Gomber, Sh. Jain, R. Khurana, M. Sharan

Tata Institute of Fundamental Research -EHEP, Mumbai, India
T. Aziz, M. Maity[5], G. Majumder, K. Mazumdar, G.B. Mohanty, K. Sudhakar

Tata Institute of Fundamental Research -HECR, Mumbai, India
S. Banerjee, S. Dugad

Institute for Research in Fundamental Sciences (IPM), Tehran, Iran
S.M. Etesami[6], A. Fahim[7], A. Jafari[7], S. Paktinat Mehdiabadi, M. Zeinali[6]

INFN Sezione di Trieste, Trieste, Italy
A. Penzo

Joint Institute for Nuclear Research, Dubna, Russia
A. Afanasyev, P. Bunin, Y. Ershov, O. Fedoseev, M. Gavrilenko, I. Golutvin, I. Gorbunov, V. Konoplynikov, A. Malakhov, P. Moisenz, V. Smirnov, A. Volodko, A. Zarubin

Institute for Nuclear Research, Moscow, Russia
Y. Andreev, A. Dermenev, N. Krasnikov, A. Pashenkov, D. Tlisov, A. Toropin

Institute for Theoretical and Experimental Physics, Moscow, Russia
V. Epshteyn, M. Erofeeva, V. Gavrilov, M. Kossov[2], I. Kudinov, N. Lychkovskaya, V. Popov, G. Safronov, S. Semenov, V. Stolin, E. Vlasov, A. Zhokin

Moscow State University, Moscow, Russia
A. Belyaev, E. Boos, M. Dubinin, L. Dudko, A. Ershov, A. Gribushin, V. Klyukhin, O. Kodolova, V. Korotkikh, I. Lokhtin, A. Markina, S. Obraztsov, M. Perfilov, S. Petrushanko, A. Popov, V. Savrin, A. Snigirev, I. Vardanyan

P.N. Lebedev Physical Institute, Moscow, Russia
V. Andreev, M. Azarkin, I. Dremin, M. Kirakosyan, A. Leonidov, G. Mesyats, A. Vinogradov

State Research Center of Russian Federation, Institute for High Energy Physics, Protvino, Russia
I. Bayshev, S. Bitioukov, V. Grishin[2], V. Krychkine, V. Petrov, R. Ryutin, A. Sobol, L. Tourtchanovitch, S. Troshin, A. Uzunian, A. Volkov

CERN, European Organization for Nuclear Research, Geneva, Switzerland
F. Santanastasio

Cukurova University, Adana, Turkey
A. Adiguzel, M.N. Bakirci[8], S. Cerci[9], C. Dozen, I. Dumanoglu, E. Eskut, S. Girgis, G. Gokbulut, E. Gurpinar, I. Hos, E.E. Kangal, G. Karapinar, A. Kayis Topaksu, G. Onengut, K. Ozdemir, S. Ozturk[10], A. Polatoz, K. Sogut[11], D. Sunar Cerci[9], B. Tali[9], H. Topakli[8], L.N. Vergili, M. Vergili

Middle East Technical University, Physics Department, Ankara, Turkey
T. Aliev, M. Deniz, A.M. Guler, A. Ozpineci, M. Serin, R. Sever, M. Zeyrek

Bogazici University, Istanbul, Turkey
M. Deliomeroglu, E. Gülmez, B. Isildak[12], M. Kaya[13], O. Kaya[13], S. Ozkorucuklu[14], N. Sonmez[15]

Istanbul Technical University, Istanbul, Turkey
K. Cankocak

National Scientific Center, Kharkov Institute of Physics and Technology, Kharkov, Ukraine
L. Levchuk

Baylor University, Waco, USA
K. Hatakeyama, H. Liu, T. Scarborough

The University of Alabama, Tuscaloosa, USA
P. Rumerio

Boston University, Boston, USA
A. Heister, C. Hill, P. Lawson, D. Lazic, J. Rohlf, St. John J, L. Sulak

Brown University, Providence, USA
G. Gennadiy, E. Laird, G. Landsberg, M. Narain, T. Sinthuprasith, K. Vang Tsang

University of California, Riverside, Riverside, USA
O.W. Long, H. Nguyen, S. Paramesvaran, J. Sturdy

University of California, Santa Barbara, Santa Barbara, USA
D. Stuart, W. To, C. West

California Institute of Technology, Pasadena, USA
A. Apresyan, Y. Chen, A. Mott, M. Spiropulu

Fairfield University, Fairfield, USA
D. Winn

Fermi National Accelerator Laboratory, Batavia, USA
S. Abdullin, J. Anderson, F. Chlebana, J. Freeman, D. Green, J. Hanlon, J. Hirschauer, U. Joshi, S. Kunori, Y. Musienko[16], S. Sharma, W.J. Spalding, S. Tkaczyk, R. Vidal, J. Whitmore, W. Wu

Florida International University, Miami, USA
V. Gaultney, S. Linn, P. Markowitz, G. Martinez

Florida State University, Tallahassee, USA
S.V. Gleyzer, S. Hagopian, V. Hagopian, M. Jenkins

Florida Institute of Technology, Melbourne, USA
M.M. Baarmand, B. Dorney, I. Vodopiyanov

The University of Iowa, Iowa City, USA
U. Akgun, E.A. Albayrak, B. Bilki[17], W. Clarida, F. Duru, J.P. Merlo, H. Mermerkaya[18], A. Mestvirishvili, A. Moeller, J. Nachtman, C.R. Newsom, E. Norbeck, J. Olson, Y. Onel, F. Ozok, S. Sen, I. Schmidt, E. Tiras, T. Yetkin, K. Yi

The University of Kansas, Lawrence, USA
R.P. Kenny III, M. Murray, J.S. Wood

University of Maryland, College Park, USA
A. Baden, B. Calvert, S.C. Eno, J.A. Gomez, T. Grassi, N.J. Hadley, R.G. Kellogg, T. Kolberg, Y. Lu, M. Marionneau, A.C. Mignerey, A. Peterman, A. Skuja, J. Temple, M.B. Tonjes

University of Minnesota, Minneapolis, USA
S.C. Kao, K. Klapoetke, J. Mans, N. Pastika

University of Mississippi, University, USA
R. Kroeger, R. Rahmat, D.A. Sanders, L. Cremaldi

State University of New York at Buffalo, Buffalo, USA
S. Jain

Northwestern University, Evanston, USA
A. Anastassov, M. Velasco, S. Won

University of Notre Dame, Notre Dame, USA
A. Heering, J. Karmgard, T. Pearson, R. Ruchti

Princeton University, Princeton, USA
E. Berry, V. Halyo, P. Hebda, A. Hunt, P. Lujan, D. Marlow, T. Medvedeva, H. Saka, C. Tully, A. Zuranski

Purdue University, West Lafayette, USA
V.E. Barnes, A.T. Laasanen

University of Rochester, Rochester, USA
A. Bodek, Y.S. Chung, P. de Barbaro, Y. Eshaq, A. Garcia-Bellido, P. Goldenzweig, J. Han, A. Harel, D.C. Miner, D. Vishnevskiy, M. Zielinski

The Rockefeller University, New York, USA
A. Bhatti, R. Ciesielski

Texas AM University, College Station, USA
W. Flanagan, T. Kamon[19], R. Montalvo, T. Sakuma

Texas Tech University, Lubbock, USA
N. Akchurin, J. Damgov, P.R. Dudero, K. Kovitanggoon, S.W. Lee, T. Libeiro, I. Volobouev

Vanderbilt University, Nashville, USA
A. Gurrola

Wayne State University, Detroit, USA
C. Milstene

Abstract

A readout box prototype for CMS Hadron Forward calorimeter upgrade is built and tested in CERN H2 beamline. The prototype is designed to enable simultaneous tests of different readout options for the four anode upgrade PMTs, new front-end electronics design and new cabling. The response of the PMTs with different readout options is uniform and the background response is minimal. Multi-channel readout options further enhance the background elimination. Passing all the electronics, mechanical and physics tests, the readout box proves to be capable of providing the forward hadron calorimeter operations requirements in the upgrade era.

[1] Now at Joint Institute for Nuclear Research, Dubna, Russia
[2] Also at CERN, European Organization for Nuclear Research, Geneva, Switzerland
[3] Also at Moscow State University, Moscow, Russia
[4] Also at Institute of Nuclear Research ATOMKI, Debrecen, Hungary
[5] Also at University of Visva-Bharati, Santiniketan, India
[6] Also at Isfahan University of Technology, Isfahan, Iran
[7] Also at Sharif University of Technology, Tehran, Iran
[8] Also at Gaziosmanpasa University, Tokat, Turkey
[9] Also at Adiyaman University, Adiyaman, Turkey
[10] Also at The University of Iowa, Iowa City, USA
[11] Also at Mersin University, Mersin, Turkey
[12] Also at Ozyegin University, Istanbul, Turkey
[13] Also at Kafkas University, Kars, Turkey
[14] Also at Suleyman Demirel University, Isparta, Turkey
[15] Also at Ege University, Izmir, Turkey
[16] Also at Institute for Nuclear Research, Moscow, Russia
[17] Also at Argonne National Laboratory, Argonne, USA
[18] Also at Erzincan University, Erzincan, Turkey
[19] Also at Kyungpook National University, Daegu, Korea

Corresponding author: Burak Bilki (Burak.Bilki@cern.ch)

1 Introduction

The Compact Muon Solenoid (CMS) [1] is a general-purpose detector designed to run at the highest luminosity provided by the CERN Large Hadron Collider (LHC). Coverage between pseudorapidities of 3.0 and 5.0 is provided by the steel/quartz fiber Hadron Forward (HF) calorimeter. The front face is located at 11.2 m from the interaction point and the depth of the absorber is 1.65 m. The signal originates from Čerenkov light emitted in the quartz fibers, which is then channeled by the fibers to photomultipliers. The absorber structure is created by machining 1 mm square grooves into steel plates, which are then diffusion welded. The diameter of the quartz fibers is 0.6 mm and they are placed 5 mm apart in a square grid. The quartz fibers, which run parallel to the beamline, have two different lengths (1.43 m and 1.65 m) which are inserted into grooves, creating two effective longitudinal samplings. The so-called "short fibers" start 22 cm inside the absorber, hence are mostly sensitive to hadron interactions. There are 13 towers in η, all with a size given by $\Delta\eta \approx 0.175$, except for the lowest-η tower with $\Delta\eta \approx 0.1$ and the highest-η tower with $\Delta\eta \approx 0.3$. The ϕ segmentation of all towers is 10°, except for the highest-η which has $\Delta\phi = 20^\circ$. This leads to 900 towers and 1800 channels in the two HF modules [2]. Details of the HF design, together with test beam results and calibration methods, can be found in [3].

The photomultiplier tubes (PMTs) of CMS HF calorimeter generate a large, fake signal when the PMT window is traversed by a relativistic charged particle due to Čerenkov light production at the PMT window. This already-known problem was observed in 2010 and 2011 data of CMS to degrade data quality and to constitute a potential to interfere with rare physics events. In the framework of CMS HF upgrade program, several types of PMTs were tested and the four-anode R7600U-200-M4 by Hamamatsu [4], was selected as the replacement PMT for the upgrade [5]. The new PMT does not only reduce the intrinsic level of background, but it also enables tagging of background events and recovering the underlying signal event (if any) by using the multi-anode features.

A readout box (RBX) prototype was built to enable the tests of different readout options for the new four anode PMTs. The new readout boards provide the flexibility to switch between four-channel, two-channel and single-channel readout of the four anode PMTs where the four-channel readout option enables the full multi-anode functionality. Both internal and external cabling of the RBX are also specific designs and selections, therefore an integral part of the prototype.

The prototype RBX was tested in CERN H2 beamline [6] in Summer-Fall 2011 with electron and muon beams to mimic calorimeter and background response respectively. Here we describe the details of certain performance tests of the RBX and report on the compatibility of the new RBX to the CMS HF upgrade framework.

2 Prototype RBX Design

The prototype RBX was built with 11 four anode PMTs in two front-end electronics boards. The boards can provide different readout options with the help of internal cabling and jumper settings. This is primarily obtained

with a two-board approach: A main base board where the PMTs are connected, and an adapter board where the signals from different anodes are combined to produce the desired readout option. Figure 1a shows a picture depicting the base and adapter boards as well as the internal cabling. PMTs are upside down on the table. The RBX can support three readout boards, only two were used in the beam tests.

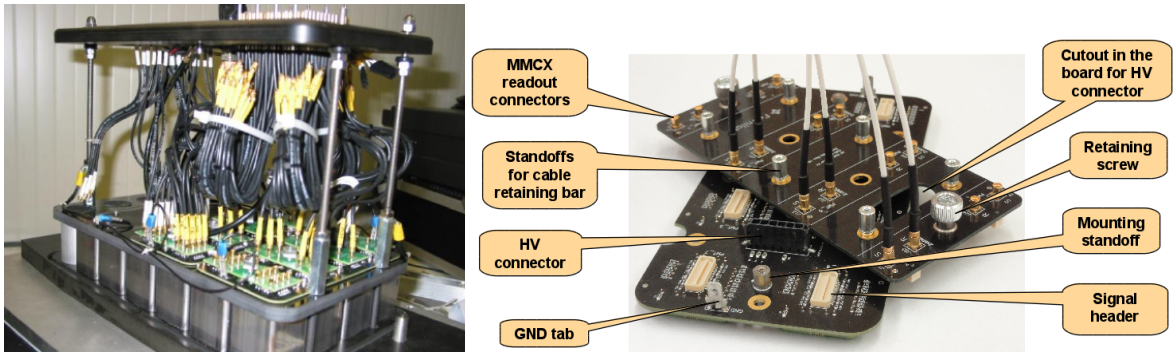

(a) (b)

Figure 1: (a) Picture depicting the prototype RBX anatomy. The PMTs are upside down on the table. The main boards, adapter boards and internal cabling are also visible. (b) Picture of the main and adapter boards before assembly. Major parts of the boards are labeled.

Readout board assembly consists of 3 major components: Base board with high voltage (HV) divider, power and safety ground connectors; PMT sockets with local dynode bypassing (installed on base boards) and adapter boards for forming any desired readout scheme (out of 4 available anodes). Figure 1b shows the readout board components.

Base board features a voltage divider design per Hamamatsu specifications [4] with a total divider resistance of 2.75 MΩ. Maximum PMT operating voltage is 900 V (330 μA for 8 PMTs). It houses bypass capacitors between all dynodes (10 nF x 200 V) and voltage divider ground connects to RBX safety ground. For better high signal rate performance, two last dynodes have boost power supply inputs: 8% and 16% of operational HV. Only photocathode HV is needed to operate at lower signal rates.

For each of the 8 PMTs on base board, a virtual ground is implemented to reduce PMT-to-PMT cross-talk and ground loop interference. All 4 PMT dynodes and their reference signals are routed to a signal header. Anode and reference circuits have bleeder resistors for HV charging prevention. Reference signals are equalized for the capacitance of PMT anode, socket, and base board artwork (additional 9 pF).

PMT socket is implemented as a sub-assembly, made of high quality gold-plated individual sockets, press-fit into a printed circuit board (PCB) with a PMT key-hole. Each PMT socket has a full set of bypass capacitors between dynodes. Last 3 dynodes have series damping resistors (50 Ω, 50 Ω and 4.7 Ω).

In order to comply with the different phases of the upgrade program, the adapter board is designed to provide convenient switching between different readout options. The adapter board uses through hole mounted MMCX signal connectors. There are screw/standoff retainers for attachment to the base board.

In the overall design of the readout boards, shortest possible connections for critical nets are used to lower series inductance. No conductors that belong to different grounds overlap. This decreases AC coupling between the grounds. The ground planes are on internal layers (i.e. against surface discharges).

3 Experimental Setup and Data Acquisition

The position of the PMTs in the RBX together with their labels used throughout this text is shown in Fig. 2. 5B, 6B, 8B, 5C and 6C are single-channel (black); 3B, 4B, 3C and 4C are two-channel (blue); 1B and 2B are four-channel (red) readout PMTs.

8B	6B	4B	2B
X	5B	3B	1B
X	6C	4C	X
X	5C	3C	X

Figure 2: The sketch of the PMTs in the RBX as seen by the beam. The labels indicate the PMT names used in this text. Color code shows single-channel (black), two-channel (blue) and four-channel (red) readout options.

The RBX was tested with 80 GeV electron and 150 GeV muon beams in the CERN H2 beamline [6] during Summer-Fall 2011 (energy and momenta units are used interchangably to describe the beam throughout the text). Figure 3 shows the two setups used for measuring the calorimetric performance and the background response of the RBX.

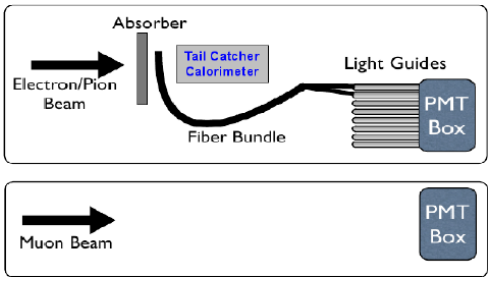

Figure 3: The sketch of the test setups for calorimeter signal (top) and muon background (bottom) measurements.

The 80 GeV electron beam was used to generate Čerenkov light through a fiber bundle. The fibers of the bundle were identical to those used in the HF. The electromagnetic shower was initiated with approximately 10 cm (6 X_0) of iron absorber. The bundle-shower crossing was downstream the absorber at 45^o angle, i.e. the bundle was at 45^o with respect to the beamline. The bundle was divided into two sections at the readout end which were inserted into the air light guides of the RBX. Therefore two PMTs could be readout simultaneously. The operating voltage for the RBX PMTs was 600 V in order to reproduce the real operating conditions of HF.

The quartz fiber calorimeter that was built for 2009 beam tests was used as a tail catcher to tag pions in the electron

beam. The calorimeter consists of 20 cm x 20 cm array of 6 mm diameter 45 cm long steel rods, and quartz fibers with similar properties to that of HF in between the rods. The fibers were bundled at the downstream end and readout with a four-anode PMT in four-channel mode.

The 150 GeV muon beam was used to generate background events on the PMT windows. For this pupose, the light guides were removed and the RBX was placed right in front of a wire chamber in order to perform precise position measurements.

The readout was performed by charge integration and encoding units (QIEs) [7] and the data was stored in CMSSW (CMS SoftWare) [8] data format. Each QIE channel was readout in 10 time slices of 25 ns each. The trigger was given by the coincidence of two scintillation counters of sizes 14 cm x 14 cm and 4 cm x 4 cm. Therefore, a beam spot of size 4 cm x 4 cm was anticipated. Another scintillation counter of size 14 cm x 14 cm was used to veto multiple particles.

For all the electron triggers, the tail catcher quartz fiber calorimeter was utilized to tag pions. Pion contamination in the electron beam was measured to be less than 1% and the pion events were not included in the analysis.

4 Fiber Bundle Characteristics

The fiber bundle was tested for signal uniformity by reading out the two ends with the same PMT in two separate electron datasets. Figure 4 shows the integrated charge profile as a function of the wire chamber coordinates for PMT 6B when it was reading out the two ends of the fiber bundle labeled A and B. The rectangles show the selection regions for the bundle location. As can be seen in the charge profiles, there are two distinct sections at the interaction end of the bundle i.e. the selection regions for the bundle locations indicate different locations in the profiles.

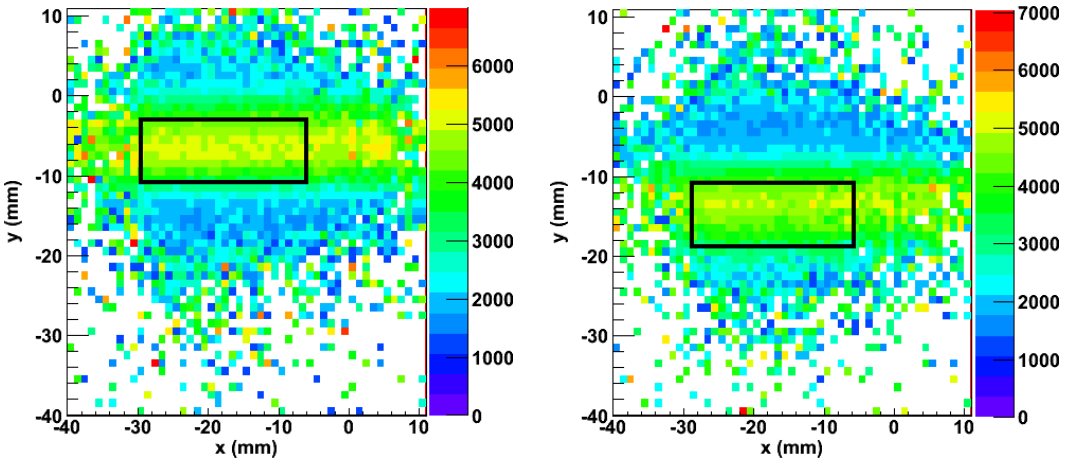

Figure 4: Integrated charge profiles for PMT 6B when it was reading A (left) and B (right) ends of the fiber bundle. Rectangles are the selection regions for the bundle location.

Figure 5 shows the number of photoelectrons distribution for PMT 6B when it was reading A (red) and B (black) ends of the bundle with the selections in Fig. 4 applied accordingly. The response of the fiber bundle is equivalent in the two readout ends. Therefore, a correction for the differences in the two readout ends is not necessary.

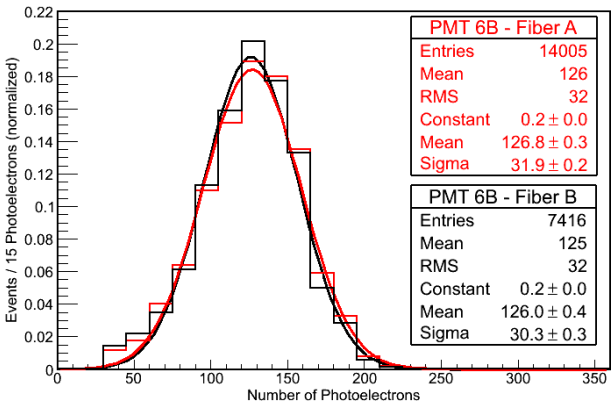

Figure 5: Signal distribution for PMT 6B when it was reading A (red) and B (black) ends. Also shown are the Gaussian fits.

5 Measurement of Multi-Channel Readout Signal Variations

The PMTs with two-channel (3B, 4B, 3C and 4C) and four-channel (1B and 2B) readout options show channel-to-channel signal variations due to various factors some of which are the intrinsic gain variations between anodes, variations in the PMT alignment in the RBX, coupling of the fiber bundle to the light guide and the variations in the light guide conditions. The overall signal for these multi-channel readout PMTs are calculated as $S = \sum c_i s_i$ where s_i (c_i) is the signal (correction factor) for each channel.

Figure 6 shows the ratio of the signal in one of the quadrants to the signal in the other quadrants for the two four-channel readout PMTs - 1B and 2B. Variations between 10 - 30 % are observed.

Figure 7 shows the ratio of the signal in one half to the signal in the other half for the four two-channel readout PMTs - 3B, 4B, 3C and 4C. Variations up to 15 % are observed.

6 Global Calibration of the RBX

Once the "per PMT" calibrations are performed, a global calibration for the entire RBX is necessary since the two-channel readout PMTs have less effective correction for multi-channel readout signal variations whereas the single-channel readout PMTs have no correction. PMT 2B is chosen as the basis for this calibration. Figure 8 shows the signal from PMT 2B (a) and 6B (b) together with the Gaussian fits. The signal for a particular PMT is corrected by a factor obtained from the ratio of the Gaussian fit mean for this PMT signal to that of PMT 2B. These correction factors imply 5 - 20 % variation between PMTs (17 % for the particular case in Fig. 8).

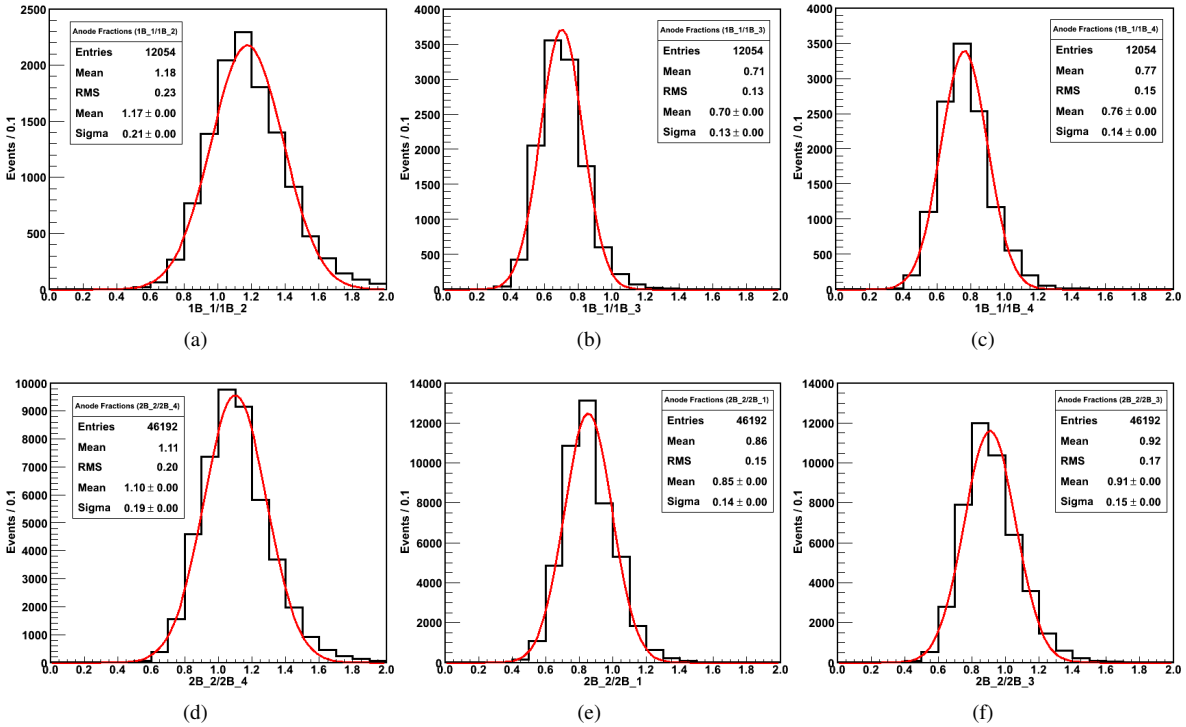

Figure 6: Ratio of the signal in one quadrant to the signal in the other quadrants for four-channel readout PMTs 1B (a, b and c) and 2B (d, e and f).

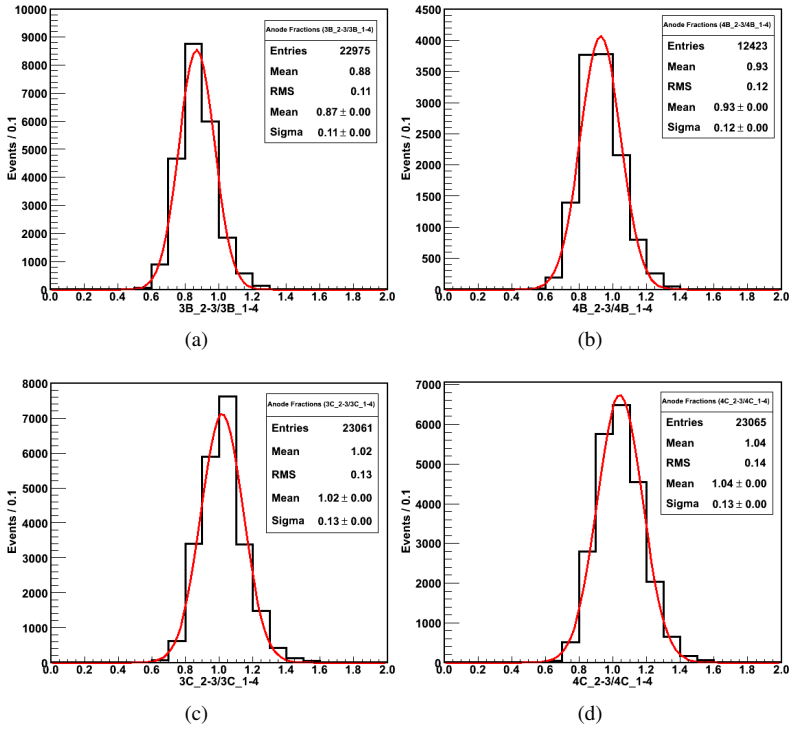

Figure 7: Ratio of the signal in one half to the signal in the other half for two-channel readout PMTs 3B (a), 4B (b), 3C (c) and 4C (d).

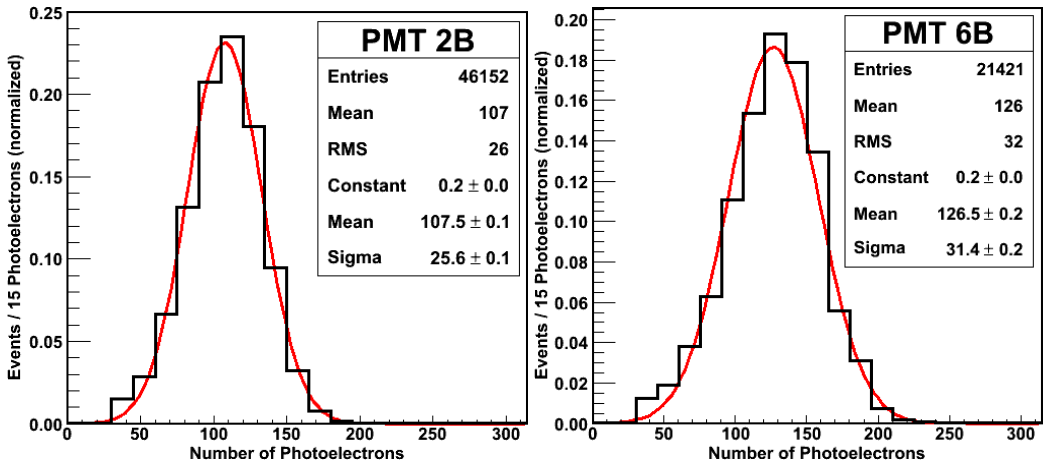

(a) (b)

Figure 8: Signal before global calibration of the RBX for PMT 2B (a) and 6B (b). 2B is a four-channel and 6B is a single-channel readout PMT.

7 Response to Čerenkov Light with the Fiber Bundle

Figure 9 shows the response of PMTs 1B - 6C (a-k) to Čerenkov light through the HF-like fiber bundle. The response over the entire RBX is uniform. A cut at 30 photoelectrons, which corresponds to about 7.5 GeV in terms of HF energy, is applied to exclude any possible MIP contribution. Overall, the signal variation within the RBX is less than 0.5 %.

8 Testing Muon Interactions with the RBX

Figure 10a shows the integrated charge profile of the entire RBX for the muon data. PMT locations are clearly visible as light green squares. In order to investigate the response of the PMTs to traversing muons, tight selections around their windows are applied. The selection region for PMT 6B is shown in Fig. 10a as a black square frame. Figure 10b shows the response of the PMTs after the window selections are applied. The response falls more than three orders of magnitude at 30 photoelectron level which corresponds to $\sim$ 7.5 GeV in HF energy units. The fraction of events above this level is $\sim 5 \times 10^{-4}$.

9 Tests of Recovery Algorithms for Background Elimination

Several algorithms to tag the background events and recover the underlying real signal (if any) were developed since Summer 2009 to comply with the progression of the upgrade program. Although all these algorithms are

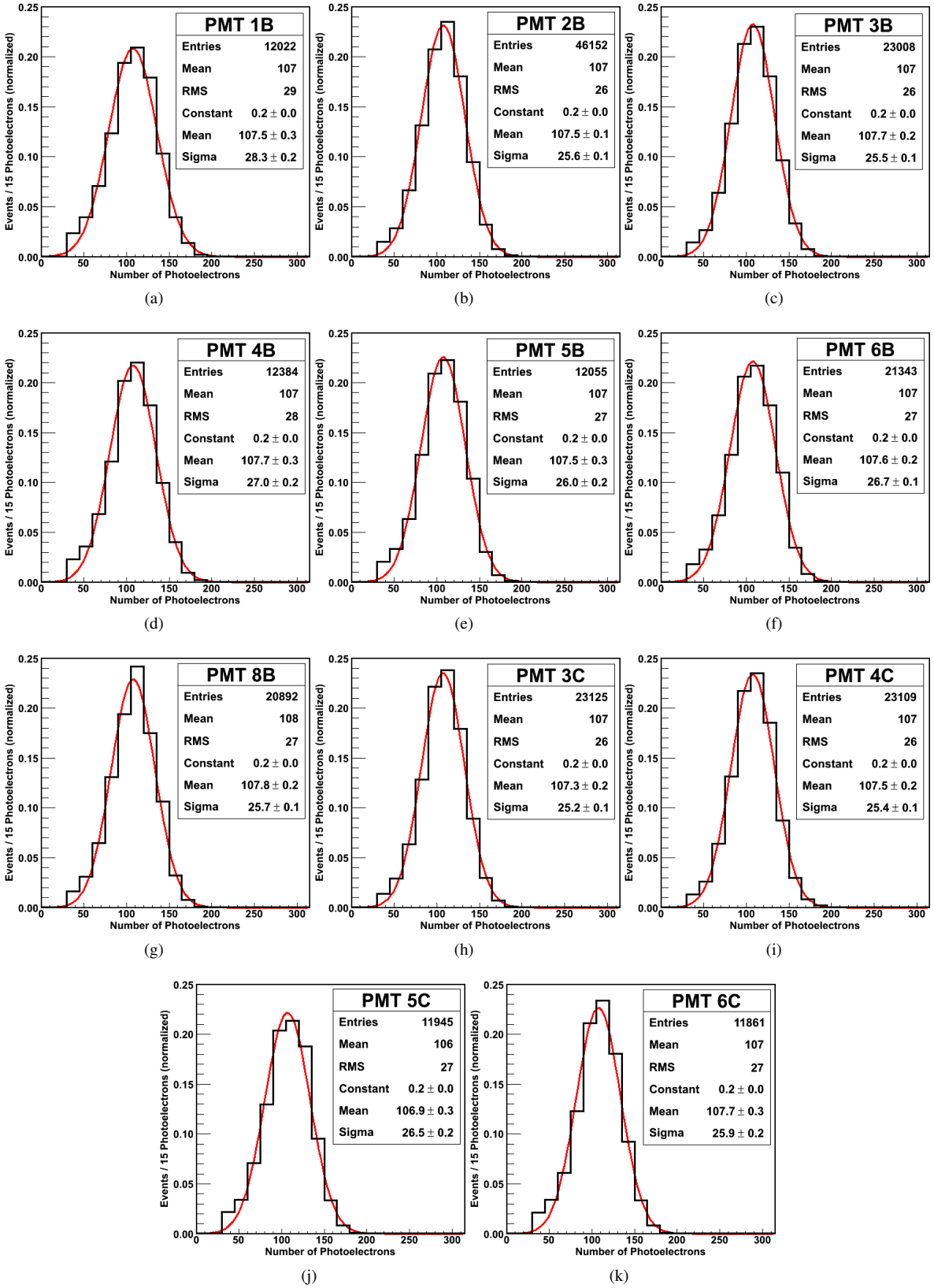

Figure 9: Response of each PMT in the RBX.

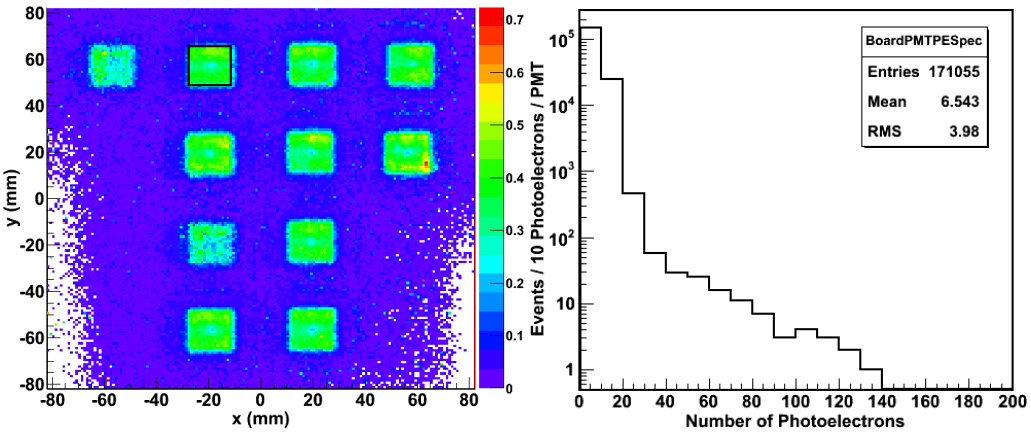

(a) (b)

Figure 10: (a) Integrated charge profile of the RBX for muons. (b) Response of the PMTs to muons traversing their windows. The fraction of events higher than 30 photoelectrons ($\sim$ 7.5 GeV HF energy) is $\sim 5 \times 10^{-4}$.

based on measuring the signal deviations between the multiple channels of the PMT, they have different systematics and efficiencies.

The four-channel readout algorithm was presented in detail in [5]. The identification of the window event is performed by observing the maximum deviation of any quadrant signal from the average quadrant signal. If this deviation is greater than the average quadrant signal, the event is tagged as a window event. Figure 11 shows the distibution of this deviation for both fiber signal (red) and muon incidence data (black). A selection at one mean deviation results in $\sim$ 98 % efficiency of window event identification. The next steps in the algorithm consist of simple tests to identify whether the deviation is due to a single or multiple quadrant hit. The unidentified 2 - 2.5 % of window hits are due to muons traversing the window close to the center. In this case, the fake signal is distributed evenly on the four quadrants as in the case of a real calorimeter signal and there is no significant deviation between the different quadrant signals. Although, this constitutes an inefficiency for the algorithm, the probability of such events is very low and the overall response of the PMT for this case is still much lower than real calorimeter signals.

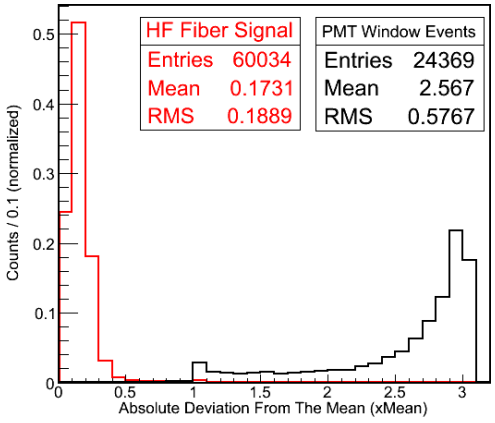

Figure 11: The distribution of the maximum absolute deviation of any quadrant signal from the mean quadrant response.

In case the four-channel readout option is not possible to implement at the first phase of the upgrade, window event tagging and signal recovery algorithms for two-channel readout option are studied in detail. There are technically two schemes to combine the signals of the four quadrants: Nearest-neighbor and cross-neighbor combination. It is obvious that the cross-neighbor combination increases the inefficiency of the tagging algorithms as the boundary between the two signal regions is maximized. Hence, the nearest neighbor combination is the viable choice.

The two-channel tagging algorithms are summarized in Table 1. The measures have 5 - 8 % inefficiency in tagging window events with the selections defined in Table 1. The distributions of these measures for the fiber signal (red) and the window events (black) in 2011 beam test data are shown in Fig. 12.

Table 1: The measures used for tagging window events in two-channel readout option. S_1 and S_2 are the signals of the two channels with $S_1 > S_2$, and $\mu = (S_1 + S_2)/2$.

Label	Measure	Window Event Selection
M1	$\frac{S_1}{S_2}$	M1>3
M2	$\frac{\sqrt{(S_1-\mu)^2+(S_2-\mu)^2}}{S_1+S_2}$	M2>0.3
M3	$\frac{S_1-\mu}{S_1+S_2}$	M3>0.25
M4	$\frac{S_1-S_2}{S_1+S_2}$	M4>0.4

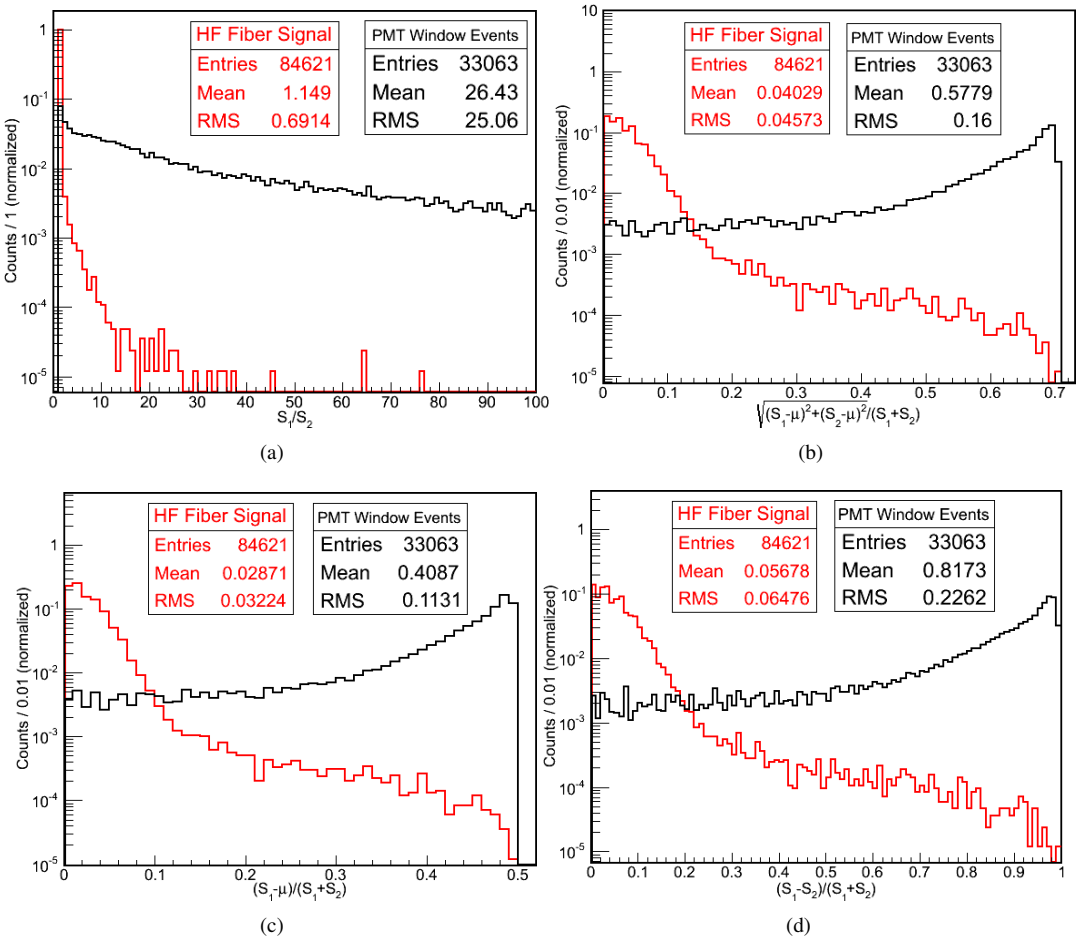

Figure 12: The distribution of the four measures in Table 1 in 2011 beam tests.

Figure 13 demonstrates the application of the four-channel algorithm and one of the two-channel algorithms (M4) to muon data. For the response larger than 30 photoelectrons, the two-channel algorithm is approximately a factor of two more inefficient than the four-channel algorithm as expected. In any case, the fraction of events larger than 30 photoelectrons remains below 2×10^{-4}.

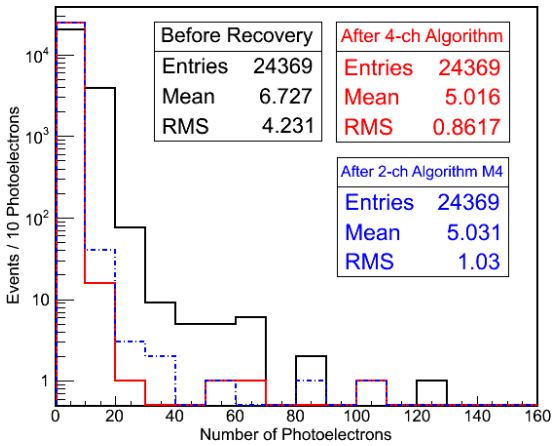

Figure 13: The results of application of the 4-ch and 2-ch M4 algorithms to muon data of 2011 beam tests.

Figure 14 shows the application of the same algorithms to the fiber bundle data of 2011 beam tests. Since the response is solely due to the Čerenkov light generated in the fiber bundle, the algorithms are expected to produce no difference in the distributions. Above 30 photoelectrons level, both algorithms result in a misidentification rate around 1×10^{-5}.

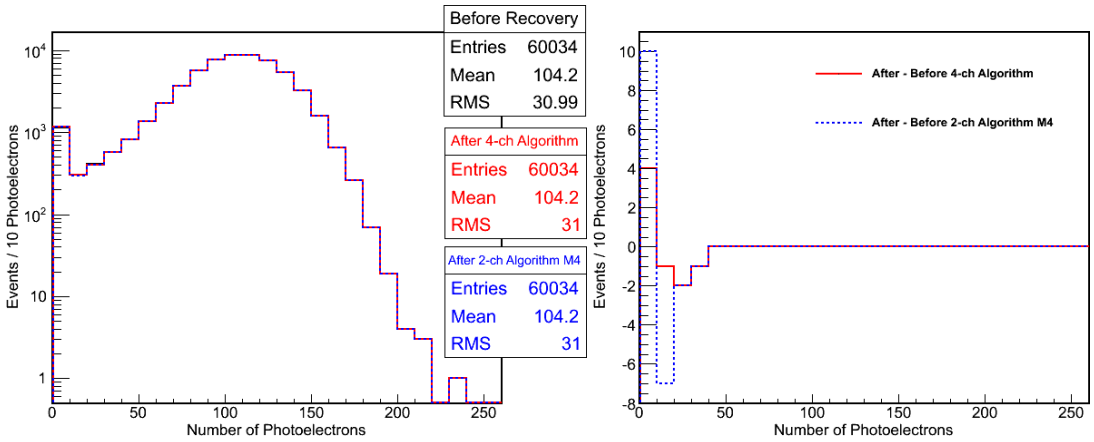

(a) (b)

Figure 14: The results of application of the 4-ch and 2-ch M4 algorithms to fiber bundle data of 2011 beam tests (a) and the differences caused by the algorithms (b).

10 Conclusions

Within the CMS HF Upgrade framework, a prototype readout box, which consists of specific designs of readout boards and cabling, and the new four-anode upgrade PMTs, was built. The readout box was extensively tested in two beam test campaigns in Summer - Fall 2011 at the CERN H2 beamline.

The readout box offers different readout options (single-channel, two-channel and four-channel) for the four anode PMT in a single compact design. During the tests, 11 four-anode PMTs were used with 5 of them in single-channel, 4 of them in two-channel and 2 of them in four-channel readout mode.

The response of the PMTs to Čerenkov light that is generated by exposing an HF-like fiber bundle in an electron shower is uniform through the entire readout box with up to 0.5 % variation.

The background response of the PMTs in the readout box is measured using muon beams. The fraction of events above 30 photoelectrons level, which corresponds to $\sim$ 7.5 GeV of HF energy, is $\sim 5 \times 10^{-4}$. This already corresponds to approximately an order of magnitude improvement on the background rate.

Several algorithms for window event tagging and signal recovery were developed for both two-channel and four-channel readout cases. On the average, the four-channel algorithm is 98% and the two-channel algorithms are 92% efficient. The fraction of events above 30 photoelectrons level is $\sim 6 \times 10^{-8}$ after four-channel and $\sim 1 \times 10^{-7}$ after two-channel algorithms. All algorithms have negligible misidentification rates.

The overall performance of the readout box is robust and reliable. All electronics, mechanical and physics tests performed on the readout box during the beam test periods were successful. The readout box is capable of providing the HF operations in the upgrade era with desired performance characteristics and flexibility to extend the readout options.

Acknowledgements

This project was carried out with financial support from U.S. Department of Energy, U.S. National Science Foundation, RMKI-KFKI (Hungary), Russian Ministry of Education and Science, Russian State Committee for Atomic Energy, Scientific and Technical Research Council of Turkey (TUBITAK), Turkish Atomic Energy Agency (TAEK) and Bogazici University Research Fund.

We thank the CERN PS and SPS accelerator personnel for their expert help in giving us excellent test beams that allowed us to carry our tests.

The data analysis was performed at the University of Iowa CMS Tier-3 computing center.

References

[1] S. Chatrchyan et al. (CMS Collabration), JINST 3, S08004, pp. 145-149 (2008).

[2] G. L. Bayatian et al. (CMS Collaboration), CERN/LHCC 2006-001 (2006).

[3] S. Abdullin et al. (CMS Collaboration), Eur. Phys. J. C 53, 1 (2008).

[4] http://www.hamamatsu.com/.

[5] S. Chatrchyan et al. (CMS HCAL Collaboration), JINST 5, P06002 (2010).

[6] http://ab-div-atb-ea.web.cern.ch/ab-div-atb-ea/BeamsAndAreas/resultbeam.asp?beamline=H2.

[7] T. Zimmerman and M. Sarraj, IEEE Trans. Nucl. Sci. 43, 1683 (1996); T. Zimmerman and J.R. Hoff, IEEE J. Solid State Circuits 39, 895 (2004).

[8] https://twiki.cern.ch/twiki/bin/view/CMS/WorkBookCMSSWFramework.